(Amount of words: 6067)

An Exploration on the Applicability of Heating Tower Heat Pump and Air Source Heat Pump Systems in Different Climatic Regions

Minzhang Liu[a,1], Lingfei Jiang[a,1], Huan Zhang[a,b], Xuejing Zheng[a,b,*], Shijun You[a,b], Shen Wei[c]

[a] School of Environmental Science and Engineering, Tianjin University, Tianjin 300350, PR China

[b] Key Laboratory of Efficient Utilization of Low and Medium Grade Energy (Tianjin University), Ministry of Education of China, Tianjin 300350, PR China

[c] The Bartlett School of Construction and Project Management, University College London (UCL), 1-19 Torrington Place, London WC1E 7HB, United Kingdom

[1] Joint First Authors

*Corresponding Author: Tel.: +08613512419172; fax: +8602227892626. E-mail addresses: zhengxuejing@tju.edu.cn

Abstract

Air source heat pump (ASHP) and heating tower heat pump (HTHP) systems are both environmentally sustainable space heating systems. HTHP system can effectively avoid the frosting issue of ASHP systems, but requires higher initial investment. In order to explore the applicability of the two systems, this paper presents a comparative study between HTHP and ASHP systems in different climatic regions. Mathematical models were developed for HTHP and ASHP systems and validated by field experiments. Case studies were carried out in four different climatic regions using the numerical model to analyze the energy consumption, system efficiency and economic efficiency of the two systems. The results showed that the ASHP system was superior in electrical power input in the four regions. The *EER* of the HTHP system was higher than that of the ASHP system by 3% and 2% in Regions III and II (Xi'an and Shanghai) while lower by 7% and 6% in Regions I and IV (Shenyang and Chongqing). The annual cost of the HTHP system was higher than that of ASHP system by 9% and 11%

in Regions I and IV, while lower by 5% and 4% in Regions II and III. Based on these comparisons, recommendations about how to choose HTHP and ASHP systems for different climatic regions were presented, to instruct future optimization and utilization of HTHP and ASHP systems.

Keywords: Heating tower heat pump; Air source heat pump; Cleaner energy; Heat and mass transfer; Energy efficiency; Climatic regions

Nomenclature

T	temperature (K)	C	annual cost(USD/y)
t	temperature (°C)		
d	specific humidity (kg_w/kg_{as})	*Subscripts*	
G	mass flow rate (kg/s)	*a*	air
h	enthalpy (kJ/kg)	*sol*	solution
c_p	specific heat at constant pressure (kJ/(kg·K))	*s*	solution surface
A	area (m^2)	*sa*	saturated
r	latent heat of evaporation of water at 0 °C (kJ/kg)	*q*	vapor
α	heat transfer coefficient(W/(m^2·K))	*r*	refrigerant
β	mass transfer coefficient (W/(m^2·K))	*ave*	floor average
Re	Reynolds number of the air	*su*	supply water
Sc	Schmidt number of the air	*re*	return water
Le	Lewis number	*H*	heating tower heat pump system
Er	criterion numeral about packing efficiency	*A*	air source heat pump system
D_G	diffusion coefficient of water vapor in the air (m^2/s)	*tp*	pump in the terminal system
a_t	specific surface area of the packing	*sp*	pump in the solution system
p	vapor pressure (Pa)	*fan*	fan
z	polytropic index		
v	specific volume (m^3/kg)	*Abbreviations*	
D_f	mean loss coefficient of the frosting and defrosting cycle	HTHP	heating tower heat pump
Q	heating capacity (kW)	ASHP	air source heat pump
P	power input (kW)	*COP*	coefficient of performance
$\overline{Q}$	ratio of the real-time heat load to the design heat load	*EER*	energy efficiency ratio

IC	initial cost(USD)	*HSPF*	heating season performance factor
RC	annual running cost(USD/y)	*RMSD*	root mean square deviation

1. Introduction

Recently, worldwide energy shortages, environment pollution and global warming are calling for clean and renewable energy. 36% of global energy consumption and nearly 40% of carbon dioxide emission are caused by building, and space heating accounts for 53% of the building energy use (International Energy Agency, 2018). How to provide comfortable indoor environment for people with minimized energy consumption has captured great attention. Air source heat pump (ASHP) and heating tower heat pump (HTHP) systems utilize low-grade thermal energy in the air and have the advantages of being pollution-free and simple to use. Therefore, these two systems have attracted a large amount of research interests.

ASHP systems have been widely used in recent decades as ideal heating sources and research on ASHP systems is relatively mature. Staffell et al. (2012) have given an overview on the characteristics, technical performance and application of ASHP systems. Using theoretical simulation, Jin et al. (2016) found that as the ambient temperature increased from −20°C to 0°C, the coefficient of performance (*COP*) of ASHP system increased from 1.92 to 2.85. The advantages of ASHP system over traditional fossil fuel heating system in efficiency and emission have been explored by researchers. In a case study carried out in a district in China, Xu et. al (2017) suggested that ASHP systems were superior to household coal or coal-fired heating boilers in terms of both thermodynamic performance and environmental impact. Mattinen et. al (2014) found in a case study in Finland that both electricity consumption and emissions

of ASHP systems were lower than those of the original district heating system. However, when an ASHP system operates in a low temperature and high humidity environment during heating seasons, frost may form and accumulate on the surface of its outdoor coils. This frost formation can degrade the system's operation performance and efficiency. It has been found that the frost formation could reduce the heating capacity and *COP* of the system by 43.4% and 40.4%, respectively (Wang et al., 2013). Vocale et al. (2014) have found that the seasonal *COP* over the whole heating season would decrease by between 1.51% and 12.67%. Although many defrosting methods, such as reverse cycle defrosting, electric heater defrosting and hot gas bypass defrosting, have been proposed to solve the issue (Song et al., 2018), they have various disadvantages, including instability, high energy demand and thermal discomfort. These shortcomings hinder the application of ASHP system in certain areas.

HTHP systems have been developed recently to address the shortcomings of the ASHP systems. Compared to ASHP system, a solution circulation system is added in the HTHP system to exchange heat with the ambient air and evaporators (Ni et al., 2015). The carrier medium in the circulation system is generally a brine solution, with a freezing point below 0°C. Therefore, HTHP systems need extra energy for the solution circulation pump compared to ASHP systems.

As a newly developed technology, studies on the thermal performance of the heating tower contributes to the understanding of the HTHP application promotion. Tan and Deng (2002, 2003) developed a heat and mass transfer numerical model for a heating tower, based on Merkel's equation (Merkel, 1925). It was derived when the Lewis number equaled one. Zhang et al. (2012) developed an analytical model for a heating tower based on a variable Lewis number, and the system's performance under different inlet parameters were analyzed in this study. Wen et al. (2012) investigated the

heat transfer coefficient in a cross-flow HTHP system using field experiments, and indicated that the air and liquid flow rates significantly affected the heat transfer coefficient. Huang et al. (2017) found the heating efficiency of heating tower varied from 10.8%~31.9%. Zendehboudi et al. (2019) studied the impact factors on the tower outlet parameters using an adaptive neuro-fuzzy inference system model. These studies have provided a theoretical foundation for predicting and improving the performance of heating towers. Liang et al. (2014) used both theoretical analysis and experimental methods to study three different regeneration modes for a heating tower solution. Huang et al. (2018) and Song et al. (2019) all developed regenerator which used low-grade heat source to study the solution regeneration, and the impacts of inlet parameters such as inlet air flow rate and temperature, inlet solution flow rate and temperature are experimentally investigated.

HTHP systems can be either open-type or closed-type (Song et al., 2017). In closed-type HTHP systems, the carrier medium flows in a coil and exchanges heat with the air indirectly, so antifreeze spray is required to prevent frost formation. Cheng et al. (2015a) founded that the antifreeze spray could improve the efficiency by 5~10% for closed-type HTHP system. In open-type HTHP systems, the carrier medium directly contacts with the ambient air. Compared to close-type HTHP, open-type HTHP systems have lower installation cost and higher efficiency, and they can also effectively solve the frosting issue. As for the efficiency of the HTHP system, Cheng et al. (2015b) found that the *COP* of HTHP was around 3.0 at the ambient air temperature of 4.3°C and relative humidity of 93.9%. Wei et al. (2016) found that the *COP* of HTHP decreased from 3.1 to 2.7 as the $CaCl_2$ mass fraction increased from 0% to 27% by experiments and an artificial neural network model. Cui et al. (2017) proposed an optimization method to improve the performance and save the investment of HTHP.

105 The existing studies have analyzed the performances of the ASHP system or the
106 HTHP systems, and provides theoretical basis for the comparison between the two
107 systems. Compared to the ASHP system, the HTHP system saves system energy
108 consumption for defrosting, but requires more energy for running an additional heat
109 exchange system. The energy consumption, system efficiency and operation cost of the
110 two systems are different, which make them suitable for different climatic conditions.
111 The comparison of HTHP and ASHP systems under different climates can provide
112 application instruction of the two systems.

113 This study has performed a comparative investigation on using HTHP and ASHP
114 systems in different climatic regions. First, heat and mass transfer model and energy
115 consumption model were built for HTHP and ASHP systems. Then, field experiments
116 were conducted to validate the models developed. Finally, a comparative analysis of
117 power input, energy efficiency and economic cost during the heating season between
118 HTHP and ASHP systems was performed in four typical climatic regions, following
119 recommendations on system selections. This study can be used to instruct future
120 optimization and utilization of HTHP and ASHP systems, and contributes to boosting
121 the application of clean energy in space heating.

122 **2. Methods**

123 **2.1. System description**

124 The schematic of the HTHP system is shown in Fig. 1. The HTHP system was
125 comprised of an open-type cross-flow heating tower, a solution pump, a heat pump
126 system and a radiant floor heating system as the indoor terminal. The refrigerant used

was R22 and the carrier medium in the heating tower was $CaCl_2$ solution.

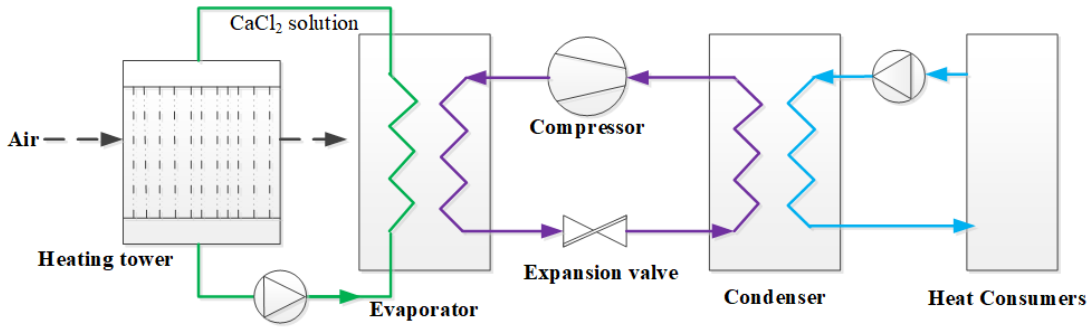

Fig. 1 Schematic of HTHP system

The schematic of the ASHP system is shown in Fig. 2. The ASHP system made up of an evaporator, a compressor, a condenser, an expansion valve and a radiant floor heating system as the indoor terminal. Reverse cycle defrosting method was adopted for the ASHP system.

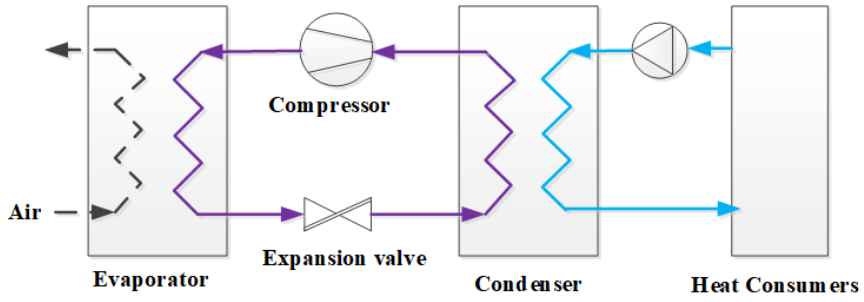

Fig. 2 Schematic of ASHP system

2.2. Model development

2.2.1. Heat and mass transfer model in the heating tower

The heat and mass transfer process between air and solution in the heating tower

is shown in Fig. 3. The solution flowed downward and was evenly distributed over the packing, while the air flowed horizontally. Then, heat and mass transfer occurred between the air and the solution.

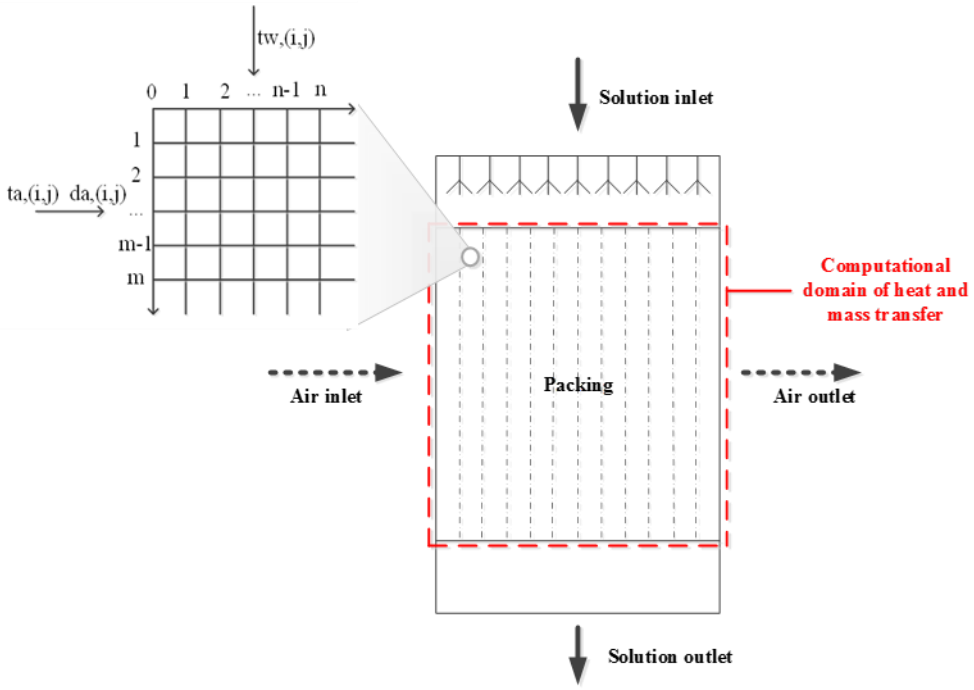

Fig. 3 Heat and mass transfer in the heating tower

The actual heat and mass transfer process is complex. Thus, the following assumptions have been made to simplify the calculation:

i) Heat and mass transfers only occurred between the air and solution;

ii) The specific heats of dry air, water vapor and solution were constant;

iii) Flow rates of air and solution were constant;

iv) The air and solution were in sufficient contact and were in thermodynamic equilibrium.

Control volumes based on the finite element method were used in this model. The

computational domain of the heat and mass transfer was subdivided into separate subsystem elements. Every control volume maintained heat and mass balance. The heat lost by the ambient air was equal to the heat gained by the $CaCl_2$ solution, as given by:

$$\frac{G_{sol}}{n} c_{p,sol} \left(T_{sol,(i+1,j)} - T_{sol,(i,j)} \right) = \frac{G_a}{m} \left(h_{a,(i,j)} - h_{a,(i,j+1)} \right) \tag{1}$$

$$\frac{G_{sol}}{n} c_{p,sol} \left(T_{sol,(i+1,j)} - T_{sol,(i,j)} \right) = \alpha_{(i,j)} \left(\frac{T_{a,(i,j)} + T_{a,(i,j+1)}}{2} - \frac{T_{sol,(i+1,j)} + T_{sol,(i,j)}}{2} \right) \frac{A}{mn} + \left(r + c_{p,q} \frac{T_{a,(i,j)} + T_{a,(i,j+1)}}{2} \right) \beta_{(i,j)} \left(\frac{d_{a,(i,j)} + d_{a,(i,j+1)}}{2} - \frac{d_{s,(i+1,j)} + d_{s,(i,j)}}{2} \right) \frac{A}{mn} \tag{2}$$

where m was the vertical partitioning grid number of the system, n was the horizontal partitioning grid number of the system.

On the other hand, the change in the air humidity was equal to the mass transferred from the $CaCl_2$ solution to the air, with the equilibrium equation as follows:

$$\frac{G_a}{m} (d_{a,(i,j)} - d_{a,(i,j+1)}) = \beta_{(i,j)} \left(\frac{d_{a,(i,j)} + d_{a,(i,j+1)}}{2} - \frac{d_{s,(i+1,j)} + d_{s,(i,j)}}{2} \right) \frac{A}{mn} \tag{3}$$

According to Djebbar and Narbaitz (1998), the empirical formula for calculating the mass transfer coefficient has been proposed as follows:

$$\beta = 0.97 (\mathrm{Re})^{0.6} (Sc)^{1.5} (Er)^{0.43} a_t D_G \tag{4}$$

The relationship between the heat and mass transfer coefficient was expressed as follows:

$$\beta = Le^{-\frac{2}{3}} \frac{\alpha}{c_p} \tag{5}$$

The Lewis number was given by the equation proposed by Klimanek and Bialecki (2009). Therefore, the convective heat transfer coefficient could be obtained by:

$$\alpha = \beta c_{\mathrm{p}} \left(0.866^{\frac{2}{3}} \frac{\frac{0.622+d_{\mathrm{s}}}{0.622+d_a} - 1}{\ln\left(\frac{0.622+d_{\mathrm{s}}}{0.622+d_a}\right)} \right)^{\frac{2}{3}} \tag{6}$$

In order to calculate the parameters related to moist air in the above equations, empirical formulas proposed by Xu (1999) were adopted. The saturated vapor pressure of moist air could be calculated from the following equations (Buck, 1981):

$$p_{sa} = 611.21 \times e^{\frac{\left(18.564 - \frac{t}{254.4}\right)t}{255.57+t}} \quad (\mathrm{t} > 0°\mathrm{C}, \mathrm{t} = 0°\mathrm{C}) \tag{7}$$

$$p_{sa} = 611.15 \times e^{\frac{\left(23.036 - \frac{t}{333.7}\right)t}{279.82+t}} \quad (\mathrm{t} < 0°\mathrm{C}) \tag{8}$$

Then the water vapor partial pressure of the $CaCl_2$ solution surface was calculated by empirical formulas proposed by Conde (2004):

$$\frac{p_s}{p_{sa}} = \lambda f(\xi, \theta) \tag{9}$$

where λ and $f(\xi,\theta)$ were parameters which can be calculated using the methods in the reference.

The equations above describe the heat and mass transfers between the air and solution in a heating tower. An iterative method has been used to solve this numerical model, with input parameters including inlet $CaCl_2$ solution temperature, dry-bulb temperature and specific humidity of the inlet air, and outputs including outlet $CaCl_2$ solution temperature, dry-bulb temperature and specific humidity of outlet air, which were determined as follows:

$$t_{sol,out} = \frac{\sum_{j=1}^{n} t_{sol,(m,j)}}{n} \tag{10}$$

$$t_{a,out} = \frac{\sum_{i=1}^{m} t_{a,(i,n)}}{m} \tag{11}$$

$$d_{a,out} = \frac{\sum_{i=1}^{m} d_{a,(i,n)}}{m} \tag{12}$$

2.2.2. Model for the heat pump systems

The following assumptions have been made in model for the heat pump systems:

i) Heat loss during the system operation was neglected;

ii) The heating capacity of the heat pump was equal to the design thermal load of the building.

The refrigerant circulation is represented in Fig. 4 by the cycle 1-2-3-4-1.

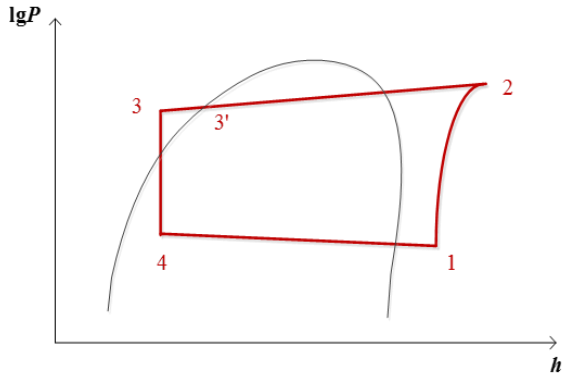

Fig. 4 P-h diagram of the vapor compression heat pump cycle

The polytropic process equation was used to describe the compression process as follows:

$$z = \frac{\ln(p_2 / p_1)}{\ln(v_1 / v_2)} \tag{13}$$

$$t_2 = t_1 (v_1 / v_2)^{z-1} \tag{14}$$

where z was the polytropic index, v_1 and v_2 were the inlet and outlet specific volume of the compressor.

The heating capacity of the condenser could be calculated by:

$$Q = G_r (h_2 - h_3) = KA(t_{a,in} - t_{a,out}) = G_{re}(t_{su} - t_{re}) \tag{15}$$

where K and A were the heat transfer coefficient and area of the building envelope, t_{in} was the indoor air design temperature, and t_{out} was the outdoor air temperature. The supply and return water temperature in the radiant floor heating system was calculated by (Chinese Standard GJ 142):

$$t_{su} = t_a + (t_{ave} - t_a)\overline{Q}^{0.969} + (t_{su} - t_{ave})\overline{Q} \tag{16}$$

$$t_{re} = t_{su} - \frac{Q}{c_{p,re} G_{re}} \tag{17}$$

The compressor power input was calculated by:

$$P = G_r (h_2 - h_1) \tag{18}$$

The enthalpy of the refrigerant was calculated using the Cleland's model (Cleland, 1986). The superheat and aftercooling degrees were chosen as 5 °C and 3 °C, respectively.

The HTHP system model could be established and calculated using the outlet parameters calculated in the heat and mass transfer model. The ASHP system model could be established by relating the evaporation temperature to the ambient air temperature (Wang et al., 2017). Then, the *COP* of the HTHP system and the ASHP

system under non-frost condition were determined by:

$$COP = \frac{Q}{P} \tag{19}$$

Under defrosting condition, the model of ASHP system needs modification.

2.2.3. Modification for the ASHP system under defrosting condition

In the defrosting process, a reverse cycle temporarily warmed up the outdoor coil to melt the frost. Based on simulations and field tests, a frosting map on the temperature–humidity chart has been proposed by Zhu et al. (2015), as shown in Fig. 5. The temperature–humidity chart was divided into three regions: a frosting region, a non-frosting region and a condensing region. Based on field tests, the reference intervals between two defrosting operation were given for all frosting zones, as listed in Table 1.

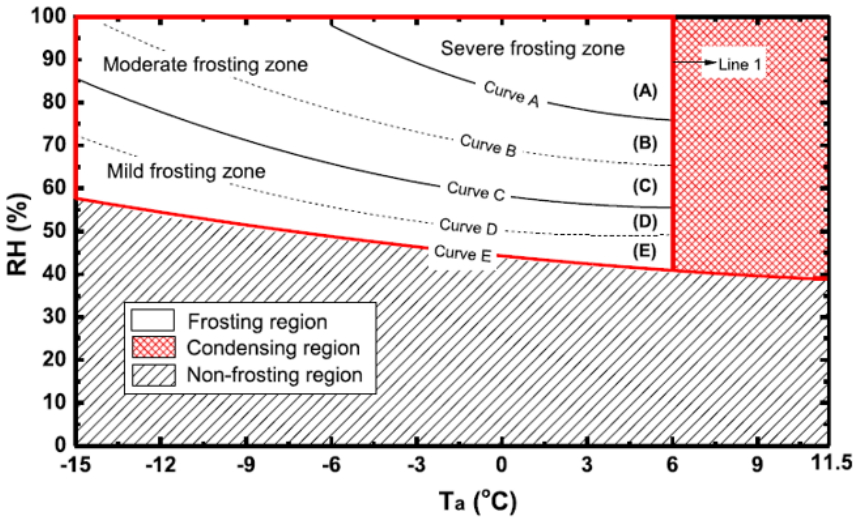

Fig. 5 Frosting map for the ASHP system (Zhu et al., 2015)

Table 1 Reference defrosting intervals for the ASHP system

Frosting zone	Reference defrosting interval (min)
A	30
B	40
C	60
D	100
E	150

221

222 The mean loss coefficient of a frosting and defrosting cycle, D_f, was proposed to
223 evaluate the influence of frosting and defrosting on the performance of the ASHP
224 system, defined as follows:

$$D_f = \frac{COP_A}{COP_{nf}} \tag{20}$$

$$COP_A = \frac{Q_{nf} t_{\text{int}} + Q_{df} t_{df}}{P_{nf} t_{\text{int}} + P_{df} t_{df}} \tag{21}$$

$$COP_{nf} = \frac{Q_{nf}}{P_{nf}} \tag{22}$$

225 where COP_A represented the modified coefficient of performance for the ASHP system;
226 COP_{nf} was the coefficient of performance under non-frosting condition; Q_{df} and P_{df}
227 were the heat supply and compressor power consumption of a standard ASHP unit
228 during the defrosting period, respectively; Q_{nf} and P_{nf} were the heat supply and
229 compressor power consumption during a non-defrosting period respectively; and t_{int}
230 was the defrosting interval. The values of D_f for different frosting zones are listed in
231 Table 2.

232 **Table 2** Mean loss coefficient of frosting and defrosting for the ASHP system

Frosting zones	D_f
A	0.64
B	0.74
C	0.80
D	0.86
E	0.91

233

234 The schematic diagram of the methodological procedure used is illustrated in Fig.

235 6.

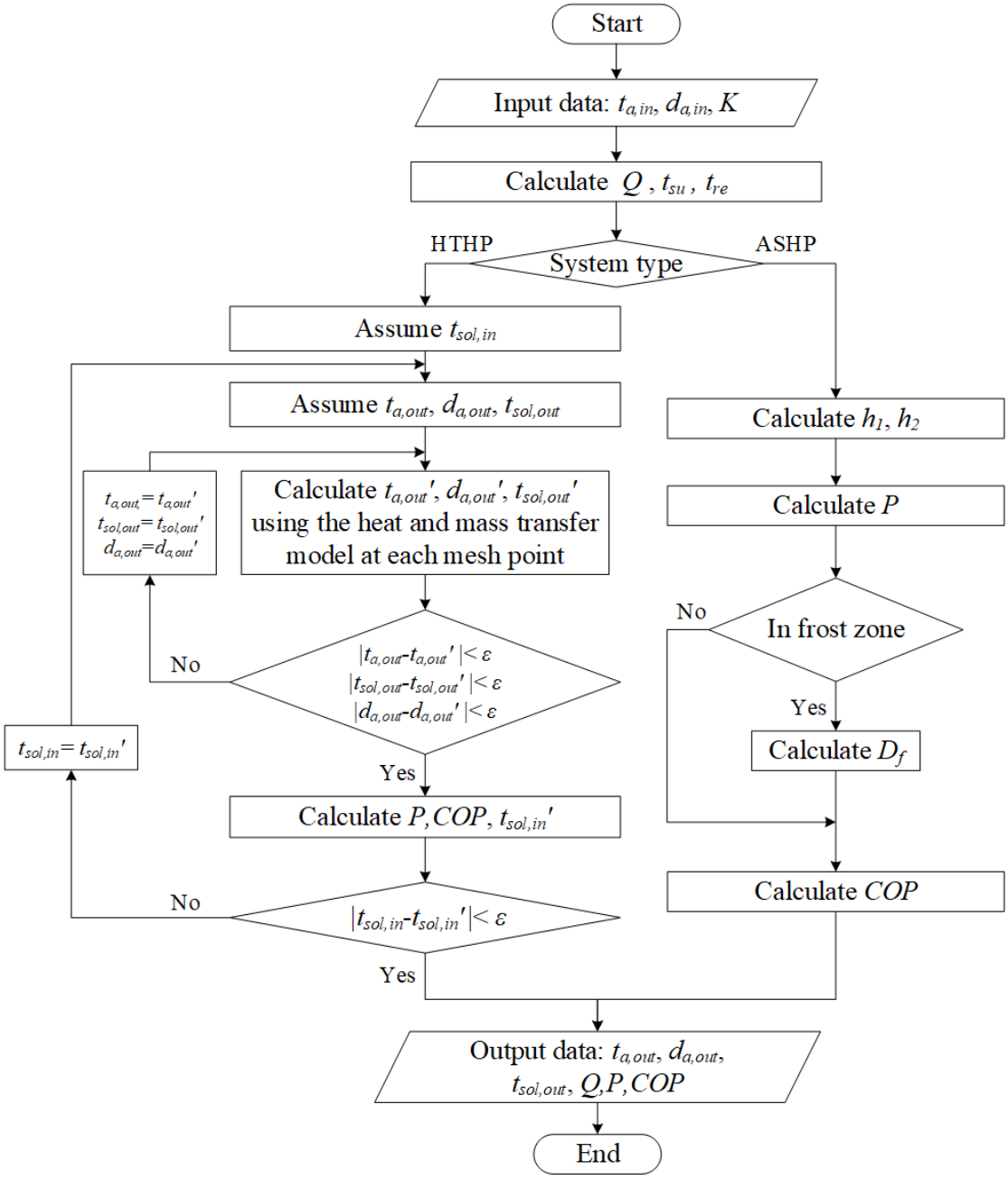

236

237 **Fig. 6** Schematic diagram of the methodological procedure

238

239 **2.3. Experimental validation**

240 2.3.1. Experimental setup

241 Experiments have been conducted to validate the numerical models. The

experimental setup for the open-type cross-flow HTHP system is shown in Fig. 7. The heating tower made up of two packings with the size of 2700mm×700mm×1800mm.

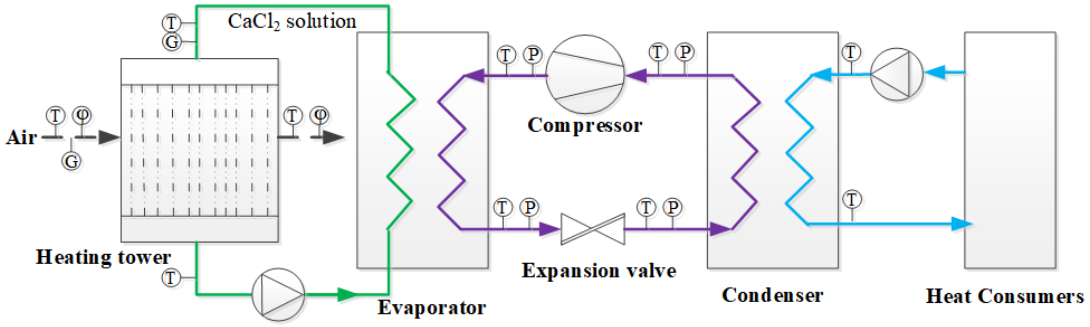

Fig. 7 Schematic of experimental setup

Two temperature and humidity sensors were installed at the air inlet and outlet to measure the dry-bulb temperature and relative humidity of the air at 10min intervals. A hot-wire anemometer was used to measure the airflow rate, and averaged value of three consecutive readings was adopted. Four thermal flow meters with Pt100 temperature sensors were used to measure the inlet and outlet temperatures of both condenser and evaporator. The mass flow rate of $CaCl_2$ solution was recorded by an ultrasonic flow meter every 20s and every ten measured data were averaged for the later analysis. The energy consumption of the compressor was recorded by a power sensor. Detailed information regarding the instruments and sensors is summarized in Table 3.

Table 3 Detailed information of the instrument and sensor

Device	Number	Accuracy	Full scale
Temperature and humidity sensor	2	±0.1°C ±1% RH	−40−100°C 0−99% RH
hot-wire anemometer	1	±3%	0−50 m/s
thermal flow meter	4	±0.1°C	−30−100°C
ultrasonic flow meter	1	±0.5%	3−18 m/h
power sensor	1	±0.5%	−

2.3.2. Uncertainty analysis

In the experiments, the uncertainties of indirect measured parameters such as Q and COP were calculated using the following equations:

$$y = f(x_1, x_2, x_3 \cdots x_n) \tag{23}$$

$$u_y = \sqrt{\sum_{i=1}^{n} \left(\frac{\partial f}{\partial x_i} u_{x_i}\right)^2} \tag{24}$$

where y was the calculated parameter correlated with independent parameters x_1, x_2, $x_3 \ldots x_n$, u_{xi} was the uncertainty for the measured parameter x_i and u_y was the uncertainty for the calculated parameter. The uncertainties of Q and COP were 3.97% and 4.17%.

2.3.3. Model validation

The inlet air and solution parameters obtained from experiments were used as the

inputs of the simulation program for calculation. The root mean square deviation (*RMSD*) has been adopted to compare the simulated and experimental results, which is calculated as follows:

$$RMSD = \sqrt{\frac{\sum\left[\left(X_{sim,i} - X_{\exp,i}\right) / X_{\exp,i}\right]^2}{n}} \tag{25}$$

Comparison between the simulation and experimental results on the outlet solution temperature, outlet air dry-bulb temperature and specific humidity are shown in Figs. 8–10.

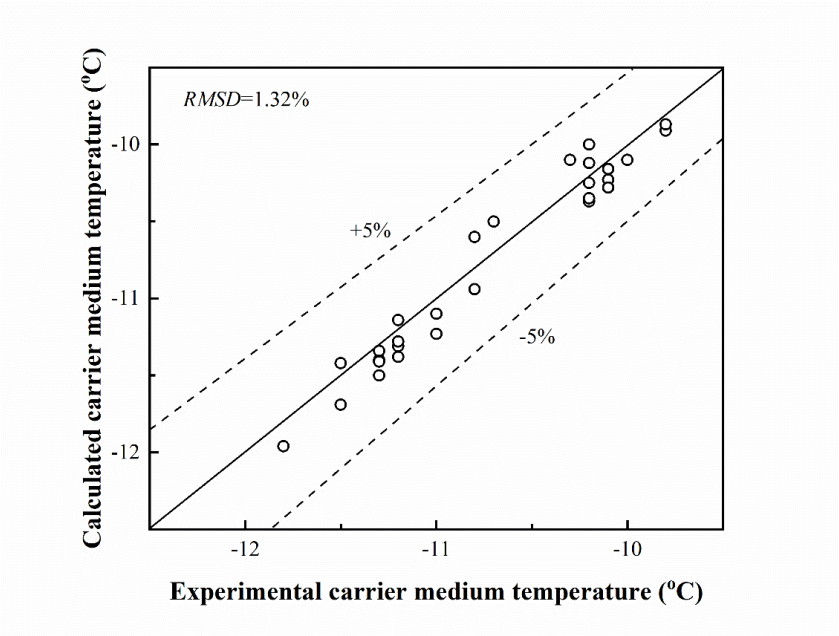

Fig. 8 Outlet carrier medium temperature for the HTHP system

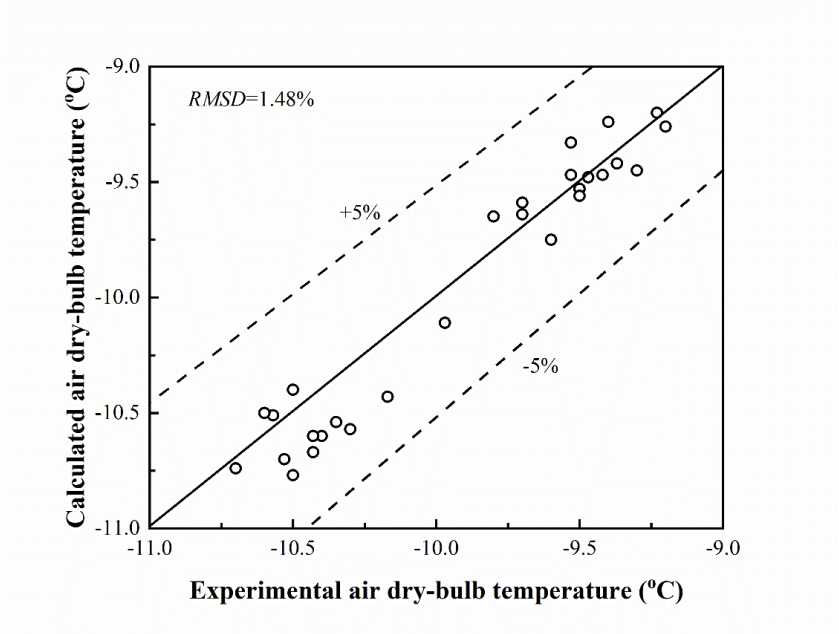

279

280 **Fig. 9** Outlet air dry-bulb temperature for the HTHP system

281

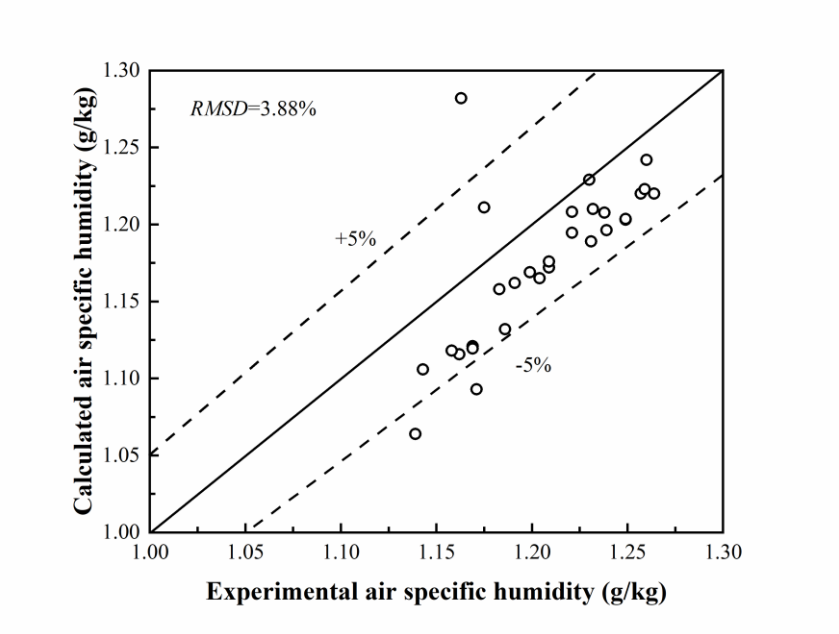

282

283 **Fig. 10** Outlet air specific humidity for the HTHP system

284

285 As shown in Figs. 8-10, over 99% of the relative errors were within 5% and all

286 were within 10%, and the *RMSD*s of the three parameters were 1.32%, 1.48% and

287 3.88%, respectively. It can be seen that the simulation results have a good agreement
288 with the experimental results, indicating that the numerical model can reflect the
289 practical operation of the system well.

290 **3. Calculation**

291 In order to analyze the applicability of both HTHP and ASHP heating systems, the
292 models established in Section 2 were applied to four different climatic regions denoted
293 as I, II, III and IV. In all these regions, the lowest recorded temperatures were below
294 0°C. The regions were divided according to the mean temperature, humidity and the
295 length of heating season. Region I represents the areas which has a severe cold and dry
296 winter, and the air temperatures are usually below 0^{o}C. Heating season of region I
297 usually lasts around 5 months. Region II has a cold and moderate humidity winter, in
298 which average temperature is below 0^{o}C. Heating season of region II usually lasts
299 around 4 months. Winter in region III is cold and humid, with an average temperature
300 above 0^{o}C. Heating season of region III is usually shorter than 3 months. In region IV,
301 winter is humid with an average temperature above 0^{o}C, and heating is necessary when
302 the temperature drops low. Climatic characteristics and worldwide representative cities
303 for the four regions have been summarized in Table 4.
304
305
306
307

Table 4 Climatic characteristics and representative cities of the four climatic regions

Region	Daily mean temperature (°C)	Monthly average low temperature (°C)	Average relative humidity (%)	Heating season length	Representative cities
I	<0	<−5	40−60	Approx. 5 months	Toronto, Havre, Shenyang
II	0−4	<0	50−70	Approx. 4 months	New York, Seoul, Xi'an
III	4−8	>0	60−80	Approx. 3 months	Atlanta, Paris, Shanghai
IV	>8	>5	>80	Less than 2 months	Wellington, Buenos Aires, Chongqing

In this study, Shenyang, Xi'an, Shanghai and Chongqing were selected as representative cities of climatic regions I, II, III and IV, respectively for calculation. The average temperatures for Shenyang, Xi'an, Shanghai and Chongqing during the heating season were −4.8°C, 3.1°C, 6.3°C and 9.1°C respectively and the average outdoor air relative humidities were 58.7%, 66.4%, 72.7% and 83.0%, respectively. The hourly outdoor air parameters of the typical meteorological year for the four cities are adopted for calculation. The time distribution of the frosting map for all four cities is listed in Table 5.

Table 5 Distribution of time in frosting map zones

City	A	B	C	D	E	Non-frosting
Shenyang	0.96%	3.21%	5.14%	36.62%	23.88%	30.19%
Xi'an	9.79%	14.91%	13.79%	22.91%	7.01%	31.48%
Shanghai	10.51%	13.80%	12.77%	20.81%	11.54%	30.57%
Chongqing	3.79%	3.64%	5.45%	1.82%	0.00%	86.06%

A three-story office building with a total floor area of 3000m^2 was analyzed in the comparative case study. The heat transfer coefficient for the building envelopes in different climatic regions depended on the local standard specifications. The calculated hourly thermal loads of the building in the four cities are shown in Fig. 11.

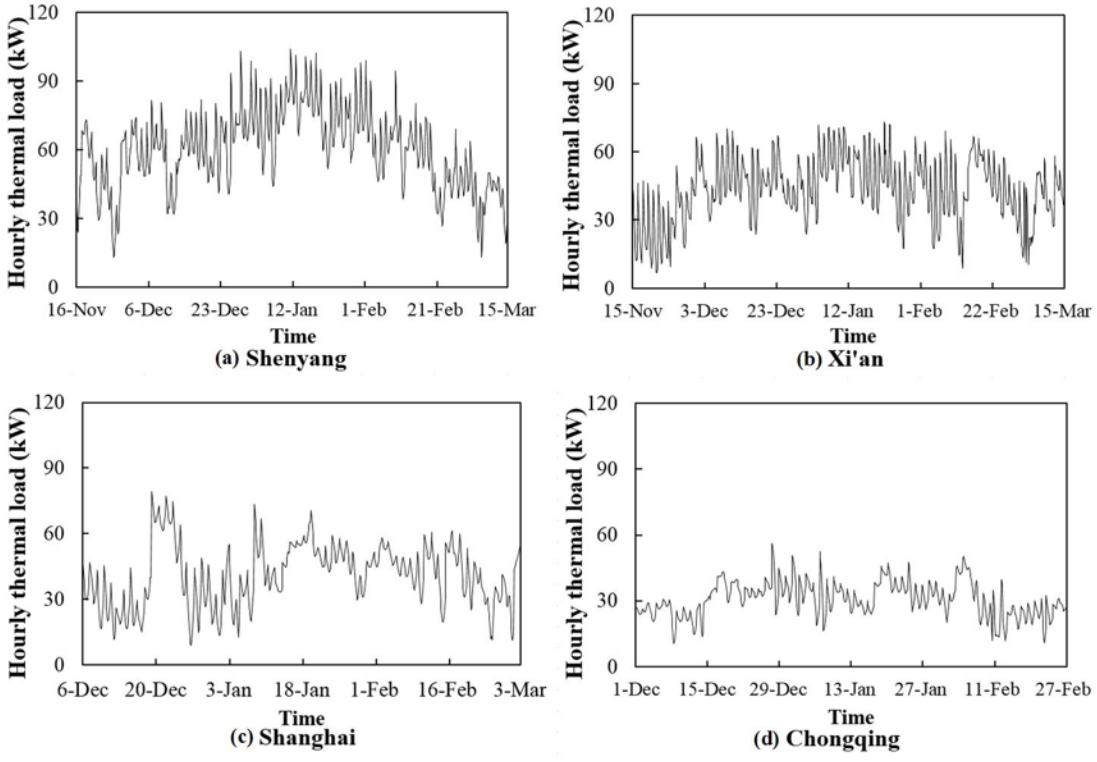

Fig. 11 Hourly thermal loads for the four cities

The energy efficiency of HTHP and ASHP systems was reflected by their *COPs*, energy efficiency ratios (*EERs*) and heating season performance factors (*HSPFs*). *COP* takes the heat capacity and energy consumption of the heat pump into account, while *EER* also considers the electricity used by the solution or air circulation and the terminal system. The *EER* was calculated as follows:

$$EER_H = \frac{Q_i}{P_{H,i} + P_{sp,i} + P_{fan,i} + P_{tp,i}} \tag{26}$$

$$EER_A = \frac{Q_i}{P_{A,i} + P_{fan,i} + P_{tp,i}} \tag{27}$$

HSPF represents the system efficiency over a whole heating season, and is defined as the ratio between the total heating capacity and the total energy consumption. *HSPF* was calculated as follows:

$$HSPF_H = \frac{\sum Q_i}{\sum\left(P_{H,i} + P_{sp,i} + P_{fan,i} + P_{tp,i}\right)} \tag{28}$$

$$HSPF_A = \frac{\sum Q_i}{\sum\left(P_{A,i} + P_{fan,i} + P_{tp,i}\right)} \tag{29}$$

4. Results and discussion

4.1. Comparison of electrical power input

As shown in Fig. 12, the hourly electrical power input of the HTHP and ASHP systems is compared. The power inputs of the HTHP system are more than that of the ASHP system for 88.4%, 74.6%, 70.7% and 92.6% of the time in Shenyang, Xi'an,

Shanghai and Chongqing, respectively. The total power inputs of the HTHP system are more than that of the ASHP system for 8.3%, 6.6%, 6.2% and 20.8% in Shenyang, Xi'an, Shanghai and Chongqing, respectively. It can be seen that although the HTHP system consumes more energy than the ASHP system over most of the time, the difference of the total power input is small for the two systems in Region I~III. The advantage of the ASHP system is more obvious in Region IV. Therefore, from the aspect of energy consumption during the heating season, ASHP system is more recommended.

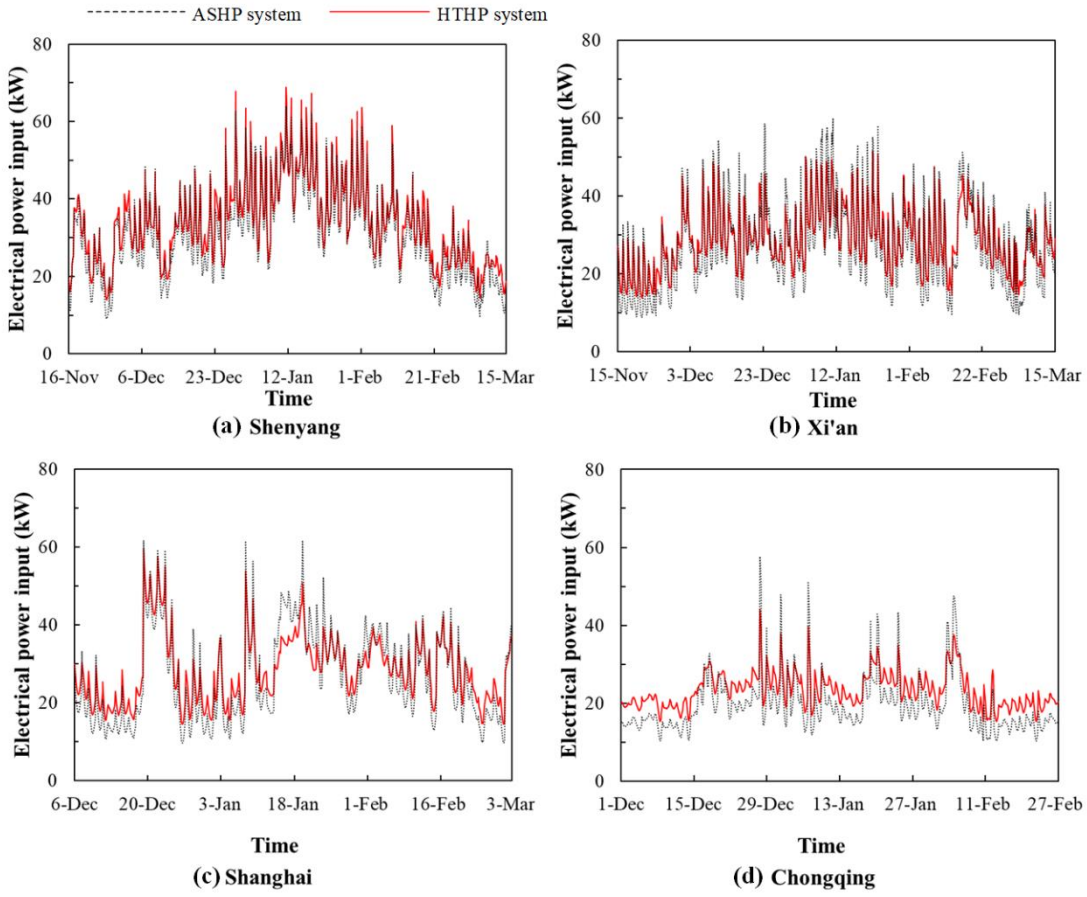

Fig. 12 Hourly electrical power input for both HTHP and ASHP systems

4.2. Comparison of energy efficiency

The averaged *COPs* of both HTHP and ASHP systems for the selected cities are shown in Fig. 13. Chongqing, Shanghai, Xi'an and Shenyang are listed in a decreasing order of *COP*. As shown in Fig. 13, the average *COP* for the HTHP system is higher than that for the ASHP system in all cities, as the ASHP system has additional energy consumption due to its defrosting system. The differences in the *COP* between the two systems are 18%, 16%, 10% and 9% for Shanghai, Xi'an, Shenyang and Chongqing, respectively. It can be deduced that the impact of the energy consumption of the defrosting system during the heating season is greatest in Shanghai and smallest in Chongqing.

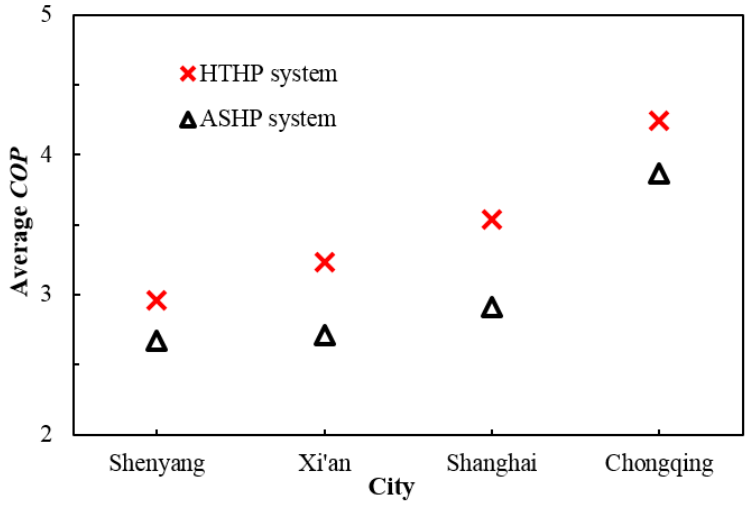

Fig. 13 Average *COPs* for both HTHP and ASHP systems

The average *EERs* and *HSPFs* for both HTHP and ASHP systems in the selected cities are shown in Fig. 14 and Fig. 15, respectively. It can be observed that a high *COP* would not necessarily correspond to a high *EER* or *HSPF*, because the latter two

370 considered the energy consumption of the whole heating system. In Shenyang, the *EER*
371 and the *HSPF* for the HTHP system are 7% and 5% lower than that for the ASHP system,
372 respectively. The reason is that although the ambient air temperature is relatively low
373 in Shenyang, the air humidity is very low as well. Therefore, frost formation will rarely
374 happen. In Chongqing, the *EER* and the *HSPF* for the HTHP system are 6% and 7%
375 lower than that for the ASHP system, respectively. This is because although the ambient
376 air humidity is high in Chongqing, the air temperature is also often high enough to
377 prevent frost. Therefore, the energy consumption of the defrosting system is relatively
378 low, and the energy consumed by the solution circulation in the HTHP system is
379 dominant. It shows that the ASHP system has an advantage in terms of energy when
380 used in Regions I and IV. In Shanghai, the *EER* and the *HSPF* for the HTHP system are
381 3% and 7% higher than that for the ASHP system, respectively. In Xi'an, the *EER* and
382 the *HSPF* of HTHP system are 2% and 7% higher than that for the ASHP system,
383 respectively. In these regions, both ambient air temperature and humidity frequently
384 meet the requirement of frosting. Therefore, the HTHP system is more suitable for
385 Regions II and III from the aspect of whole system efficiency.

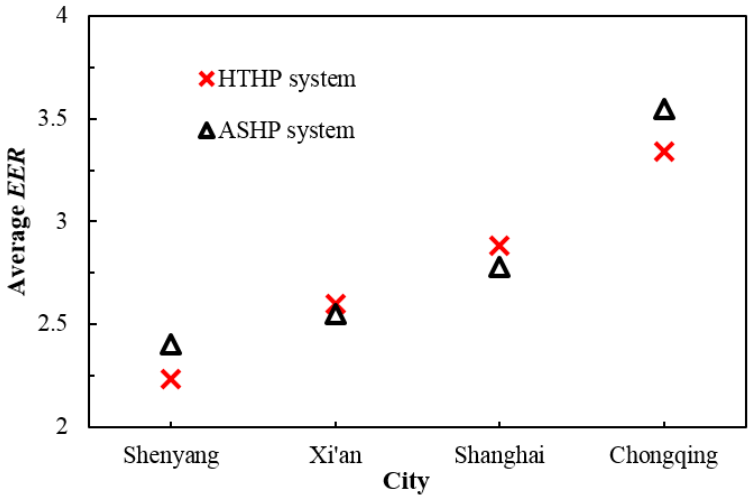

386

387 **Fig. 14** Average *EERs* for both HTHP and ASHP systems

388

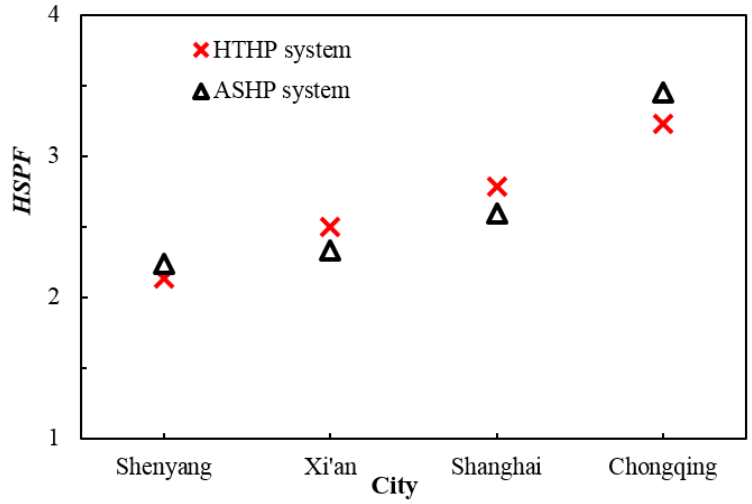

389

390 **Fig. 15** *HSPFs* for both HTHP and ASHP systems

391

392 **4.3. Comparison of economic efficiency**

393 The annual cost has been introduced to analyze the economic applicability of the

394 HTHP and ASHP systems during the heating season for the selected cities. The annual

395 cost included initial cost and running cost. The unit prices per kilowatt which were

obtained from engineering estimation method are listed in Table 6. For the HTHP system, the price of the heating tower, solution pump and supplement of $CaCl_2$ solution were also considered. The initial cost was calculated by the unit prices and the building loads of the four cities. The running cost were calculated by the total electricity consumption and the electricity price during the heating season.

Table 6 Unit prices used in the calculation of initial cost

ASHP system		HTHP system	
Item	Unit Price (USD/kW)	Item	Unit Price (USD/kW)
ASHP system equipment set	190	HTHP system equipment set	240
Capacity supplementing fee	70	Capacity supplementing fee	70
Radiant floor heating system	85	Radiant floor heating system	85

The annual cost of the system was calculated by static evaluation and it was defined as follows:

$$C = \frac{IC}{n} + RC \tag{30}$$

where the life cycle, n, was calculated as 20 years.

A comparison in terms of economic efficiency between HTHP and ASHP systems is summarized in Table 7.

411 **Table 7** Economic cost of HTHP and ASHP systems in four cities

City	HTHP system			ASHP system			$(C_H-C_A)/C_A$
	Initial cost IC_H (USD)	Annual running cost RC_H (USD/y)	Annual cost C_H (USD/y)	Initial cost IC_A (USD)	Annual running cost RC_A (USD/y)	Annual cost C_A (USD/y)	
Shenyang	40685	5642	7676	35535	5208	6985	9%
Xi'an	29230	4218	5680	25530	4671	5948	-5%
Shanghai	31600	3177	4757	27600	3575	4955	-4%
Chongqing	22120	2584	3960	19320	2365	3331	11%

412

413 As can be seen, the initial cost of HTHP system is higher than that of ASHP system
414 in all four cities, resulted from the additional heating tower and solution pump. The
415 annual costs of HTHP system are lower by 5% and 4% than that of ASHP system in
416 Xi'an and Shanghai, respectively. Whereas, in Shenyang and Chongqing, the HTHP
417 system has a higher annual cost than the ASHP system. Both ambient air temperature
418 and humidity in Region I are relatively low, but relatively high in Region IV. In these
419 areas, the ASHP system has rare frost cases. Therefore, the ASHP system is more
420 suitable in Regions I and IV. However, winter is humid in Region II and III. Frosting
421 for ASHP system is serious in these places, resulting in a high running cost for
422 defrosting. Therefore, HTHP systems have a comparative advantage in Regions II and
423 III in terms of economic costs.

5. Conclusion

ASHP and HTHP systems can both collect heat from ambient air and transfer it into buildings. These two systems, however, have different energy consumption patterns. This study is aimed to compare the performance characteristics of both systems during heating seasons in order to provide reference for future application. The electrical power input, *COP*, *EER*, *HSPF* and annual cost for both systems are compared for four different climatic regions using numerical models. This study will expand the application area of both systems. In the future, the annual performances of both systems can be investigated for other climatic regions using the method proposed in this study. And a reference for the system selection in various regions of the world will be provided. The major conclusions from this study can be summarized as follows:

(1) The total electrical power inputs of the HTHP system are higher than that of the ASHP system by 8.3%, 6.6%, 6.2% and 20.8% in Regions I, II, III and IV, respectively. This indicates that ASHP system is superior in the electrical power input, particularly in Regions IV.

(2) The average *COPs* of the HTHP system are higher than that of the ASHP system in all regions, and the differences are 18%, 16%, 10% and 9% in Regions III, II, I and IV, respectively. The average *EERs* of the HTHP system are lower than that of the ASHP system by 7% and 6% in Regions I and IV, but higher than that of the ASHP system by 3% and 2% in Regions III and II. Therefore, in term of system efficiency, HTHP system is more recommended than ASHP system in Regions II and III, whereas

it is the opposite in Regions I and IV.

(3) In Regions I and IV, the annual costs of the HTHP system are higher than that of the ASHP system by 9% and 11%, respectively. In Regions II and III, the running costs of the HTHP system are lower than that of the ASHP system by 5% and 4%, respectively. Therefore, it is recommended to use HTHP systems for Regions II and III, and ASHP systems are more suitable for Regions I and IV from the aspect of economical cost.

Acknowledgment

The study has been supported by the China National Key R&D Program (Grant No. 2016YFC0700104).

Reference

Buck, A.L., 1981. New equations for computing vapor pressure and enhancement factor. Journal of applied meteorology. Journal of Applied Meteorology 20(12), 1527-1532. https://doi.org/ 10.1175/1520-0450(1981)020<1527:NEFCVP>2.0.CO;2

Cheng, J., Li, N., Wang, K., 2015a. Study of Heat-source-Tower Heat Pump System Efficiency. Procedia Engineering 121, 915-921. https://doi.org/10.1016/j.proeng.2015.09.050

Cheng, J., Zou, S., Chen, S., 2015b. Application Research on the Closed-loop Heat-source-Tower Heat Pump Air Conditioning System in Hot-summer and Cold-winter Zone. Procedia Engineering 121, 922-929. doi:

https://doi.org/10.1016/j.proeng.2015.09.051

Chinese Standard GJ 142, 2012. Technical specification for radiant heating and cooling.

Cleland, A.C., 1986. Computer subroutines for rapid evaluation of refrigerant thermodynamic properties. International Journal of Refrigeration 9(6), 346-351. https://doi.org/10.1016/0140-7007(86)90006-X

Conde, M.R., 2004. Properties of aqueous solutions of lithium and calcium chlorides: formulations for use in air conditioning equipment design. Int J Therm Sci 43(4), 367-382. https://doi.org/10.1016/j.ijthermalsci.2003.09.003

Cui, H.J., Li, N.P., Wang, X.L., Peng, J.Q., Li, Y., Wu, Z.B., 2017. Optimization of reversibly used cooling tower with downward spraying. Energy 127, 30-43. https://doi.org/10.1016/j.energy.2017.03.074

Djebbar, Y., Narbaitz, R.M., 1998. Improved Onda correlations for mass transfer in packed towers. Water science and technology 38(6), 295-302. https://doi.org/10.2166/wst.1998.0264

Huang, S.F., Lv, Z.Y., Liang, C.H., Zhang, X.S., 2017. Experimental study of heat and mass transfer characteristics in a cross-flow heating tower. Int J Refrig 77, 116-127. https://doi.org/10.1016/j.ijrefrig.2017.02.020

Huang, S.F., Lv, Z.Y., Zhang, X.S., Liang, C.H., 2018. Experimental investigation on heat and mass transfer in heating tower solution regeneration using packing tower. Energ Buildings 164, 77-86. https://doi.org/10.1016/j.enbuild.2017.12.064

International Energy Agency, 2018. Global status report: towards a zero-emission,

efficient and resilient buildings and construction sector.

Jin, L., Cao, F., Yang, D.F., Wang, X.L., 2016. Performance investigations of an R404A air-source heat pump with an internal heat exchanger for residential heating in northern China. Int J Refrig 67, 239-248. https://doi.org/10.1016/j.ijrefrig.2016.03.004

Klimanek, A., Bialecki, R.A., 2009. Solution of heat and mass transfer in counterflow wet-cooling tower fills. Int Commun Heat Mass 36(6), 547-553. https://doi.org/10.1016/j.icheatmasstransfer.2009.03.007

Liang, C.H., Wen, X.T., Liu, C.X., Zhang, X.S., 2014. Performance analysis and experimental study of heat-source tower solution regeneration. Energ Convers Manage 85, 596-602. https://doi.org/10.1016/j.enconman.2014.05.020

Mattinen, M.K., Heljo, J., Vihola, J., Kurvinen, A., Lehtoranta, S., Nissinen, A., 2014. Modeling and visualization of residential sector energy consumption and greenhouse gas emissions. J Clean Prod 81, 70-80. https://doi.org/10.1016/j.jclepro.2014.05.054

Merkel, F., 1925. Verdunstungskühlung. VDI-Verlag.

Ni, L., Dong, J.K., Yao, Y., Shen, C., Qv, D.H., Zhang, X.D., 2015. A review of heat pump systems for heating and cooling of buildings in China in the last decade. Renew Energ 84, 30-45. https://doi.org/10.1016/j.renene.2015.06.043

Song, M.J., Deng, S.M., Dang, C.B., Mao, N., Wang, Z.H., 2018. Review on improvement for air source heat pump units during frosting and defrosting. Appl

Energ 211, 1150-1170. https://doi.org/10.1016/j.apenergy.2017.12.022

Song, P., Li, X., Wang, B., Shi, W., 2017. Experimental Study on Solution Regeneration Performance of Closed-type Heat-source Tower. Procedia Engineering 205, 446-452. https://doi.org/10.1016/j.proeng.2017.10.396.

Song, P., Xiao, H., Wang, B., Shi, W., Li, X., Zhang, G., 2019. Experimental investigation of the regeneration performance of an internally heated regenerator used for heating tower solution regeneration. Energ Convers Manage 189, 184-194. https://doi.org/10.1016/j.enconman.2019.03.089

Staffell, I., Brett, D., Brandon, N., Hawkes, A., 2012. A review of domestic heat pumps. Energ Environ Sci 5(11), 9291-9306. https://doi.org/10.1039/C2EE22653G

Tan, K.X., Deng, S.M., 2002. A method for evaluating the heat and mass transfer characteristics in a reversibly used water cooling tower (RUWCT) for heat recovery. Int J Refrig 25(5), 552-561. https://doi.org/10.1016/S0140-7007(01)00044-5

Tan, K.X., Deng, S.M., 2003. A numerical analysis of heat and mass transfer inside a reversibly used water cooling tower. Build Environ 38(1), 91-97. https://doi.org/

Vocale, P., Morini, G.L., Spiga, M., 2014. Influence of Outdoor Air Conditions on the Air Source Heat Pumps Performance. Energy Procedia 45, 653-662. https://doi.org/10.1016/j.egypro.2014.01.070

Wang, B.L., Liu, X.R., Shi, W.X., 2017. Performance improvement of air source heat pump using gas-injected rotary compressor through port on blade. Int J Refrig 73,

91-98. https://doi.org/10.1016/j.ijrefrig.2016.09.017

Wang, W., Feng, Y.C., Zhu, J.H., Li, L.T., Guo, Q.C., Lu, W.P., 2013. Performances of air source heat pump system for a kind of mal-defrost phenomenon appearing in moderate climate conditions. Appl Energ 112, 1138-1145. https://doi.org/10.1016/j.apenergy.2012.12.054

Wei, X.Q., Li, N.P., Peng, J.Q., Cheng, J.L., Su, L., Hu, J.H., 2016. Analysis of the Effect of the CaCl2 Mass Fraction on the Efficiency of a Heat Pump Integrated Heat-Source Tower Using an Artificial Neural Network Model. Sustainability-Basel 8(5). https://doi.org/10.3390/su8050410

Wen, X.T., Liang, C.H., Zhang, X.S., 2012. Experimental study on heat transfer coefficient between air and liquid in the cross-flow heat-source tower. Build Environ 57, 205-213. https://doi.org/10.1016/j.buildenv.2012.03.004

Xu, C., Wang, C.L., Xu, G., Hu, Y., Guo, H., Yang, Y.P., 2017. Thermodynamic and environmental evaluation of an improved heating system using electric-driven heat pumps: A case study for Jing-Jin-Ji region in China. J Clean Prod 165, 36-47. https://doi.org/10.1016/j.jclepro.2017.07.087

Xu, S.H., 1999. Equations for calculating thermophysical properties of moist air. Journal of Suzhou University 15(3).

Zendehboudi, A., Song, P.Y., Li, X.T., 2019. Performance investigation of the cross-flow closed-type heat-source tower using experiments and an adaptive neuro-fuzzy inference system model. Energ Buildings 183, 340-355.

https://doi.org/10.1016/j.enbuild.2018.11.003

Zhang, Q., Wu, J.S., Zhang, G.Q., Zhou, J., Guo, Y.H., Shen, W., 2012. Calculations on performance characteristics of counterflow reversibly used cooling towers. Int J Refrig 35(2), 424-433. https://doi.org/10.1016/j.ijrefrig.2011.10.016

Zhu, J.H., Sun, Y.Y., Wang, W., Ge, Y.J., Li, L.T., Liu, J.D., 2015. A novel Temperature-Humidity-Time defrosting control method based on a frosting map for air-source heat pumps. Int J Refrig 54, 45-54. https://doi.org/10.1016/j.ijrefrig.2015.02.005